Effect of Cation Substitution on the $TaTe_2$ Distortion

Stephen Lee* and N. Nagasundaram

Department of Chemistry, University of Michigan, Ann Arbor, Michigan 48109

Received June 23, 1989

We report the preparation of the new substituted phases $Ta_xM_{1-x}Te_2$ (for M = Ti, Nb $0 \leq x \leq 1$; for Zr $x > 0.5$; for Hf $x > 0.875$). We study the effect of the disorder introduced by cation substitution on the $TaTe_2$ distortion of the CdI_2 structure type. Disorder effects due to the size of the substituting cation are found to be of minor importance to the distortion. Electronic factors however play a major role.

Octahedrally coordinated transition-metal dichalcogenides present to the solid-state chemist one of the richest collections of variations on a structural theme. The theme is the CdI_2 structure (1T type), shown in Figure 1.[1] This structure is a hexagonal closest packing of the anions in which half the octahedral holes are occupied, forming alternate layers of completely filled and empty octahedra. The variations include the $TaTe_2$, high-temperature $MoTe_2$, WTe_2, $ReSe_2$, $AuTe_2$, $AgAuTe_4$, $TaSe_2$, and $Ta_{1-x}Ti_xS_2$ structure types.[2] This myriad of types all involve different clusterings of the metal atoms of a single layer with concomitant formation of metal–metal bonds of varying strengths.

In examining the different structures, one finds there is often a division between the sulfur and selenium compounds on one hand and the tellurides on the other. For example 1T-TaS_2 and -$TaSe_2$ both distort in the same manner from the original CdI_2 structure type, while $TaTe_2$ distorts in an entirely different way.[2a,g] Another example of this division is found with tungsten. No 1T-WS_2 or 1T-WSe_2 is known, while WTe_2 forms a distorted 1T of a unique type.[3] Similar differences can be found for niobium, nickel, and gold.[4]

Much of the recent work has been concerned primarily with the sulfides and selenides.[5] As the above discussion shows, the tellurides have an interesting chemistry all of their own. In this article we concentrate on the $TaTe_2$ structure type, which is known only for the tellurides, VTe_2, $NbTe_2$, and $TaTe_2$.[2a,h] This is a monoclinic distortion of CdI_2 (although it has a centered rectangular cell with respect to a single octahedral layer). The tantalum atoms distort to form the triple tantalum chain shown in Figure 2. The shortest Ta–Ta distance is 3.32 Å, while the separation between Ta atoms of different chains is 4.51 Å, and hence the distortion is considerable. This shortest distance is comparable in length to the longer bonds found in elemental Ta (six longer bonds at 3.30 Å and eight shorter 2.86-Å bonds[6]).

Table I. Guinier Powder Pattern for $Ta_{0.8}Zr_{0.2}Te_2$

h,k,l	d_{obs}, Å	d_{calc}, Å	I_{obs}	I_{calc}[a]
0,0,1	6.71	6.72	s	24.7
0,0,2	3.361	3.362	mw	2.9
1,0,1	2.902	2.903	vs	100.0
1,0,2	2.3242	2.3248	vs	58.3
0,0,3	2.2409	2.2411	m	6.8
1,1,0	1.8582	1.8582	ms	32.8
1,0,3	1.8392	1.8392	m	20.5
1,1,1	1.7919	1.7910	m	5.4
0,0,4	1.6814	1.6808	ms	7.1
1,1,2	1.6274	1.6263	w	2.2
2,0,1	1.5648	1.5650	mw	19.0
2,0,2	1.4514	1.4515	wm	16.4
1,1,3	1.4301	1.4305	wvw	12.2
1,0,5	1.2406	1.2407	wm	12.7
2,1,0	1.2164	1.2165	w	1.4

[a] As calculated by the LAZY PULVEVIX program of K. Yvon, W. Jeitschko, and E. Parthé.

We have studied the effect of the substitution of other atoms into the $TaTe_2$ host to form compounds of the form $Ta_xM_{1-x}Te_2$ (M = Ti, Zr, Hf, V, and Nb). Our work shows that the effect due to the size of the substituted cation is rather unimportant to the formation of the distorted $TaTe_2$ phase. Electronic factors play a more dominant role.

Experimental Section

All samples were prepared from stoichiometric mixtures of the elements. Nominal purities were for Ti 99.9%, Hf 99.5%, Ta 99.9%, Te 99.99% (all from Aldrich), Zr 99.9%, Nb 99.8%, and V 99.7% (all from Alfa). Metal particle size was found to be important. The most homogeneous results were obtained when the transition-metal powder was −60 mesh and generally −325 mesh metal powders were used. We placed 1–2-g samples in sealed, evacuated fused quartz tubes and heated them slowly (100–200 °C/day) to 1070 °C. They were annealed at this temperature for 2 days, after which the furnace was turned off. The tubes were removed 5–10 h later when the furnaces had reached room temperature. Room-temperature Guinier photographs (Enraf-Nonius, Cu $K\alpha_1$ radiation, λ = 1.540 56 Å, Ge standard, a = 5.6580 Å) were taken. In many cases the samples were further examined by electron microprobe to ensure the homogeneity and purity of the products (Cameca MBX automated electron microprobe with Kevex 8000 microanylser applied to single crystals).

Results

The $Ta_xM_{1-x}Te_2$ (M = Ti, Zr, Hf, V, and Nb) generally crystallized in either the CdI_2 or $TaTe_2$ structure types.

(1) The IT type is the simplest of the CdI_2 allotropes. See: Bozorth, R. M. *J. Am. Chem. Soc.* **1922**, *44*, 2232.

(2) (a) $TaTe_2$: Brown, B. E. *Acta Crystallogr.* **1966**, *20*, 264. Van Landyt, J.; Van Tendeloo, G.; Amelinckx, S. *Acta Crystallogr.* **1975**, *A31*, S85. (b) $MoTe_2$ (high temperature) and WTe_2: Brown, B. E. *Acta Crystallogr.* **1966**, *20*, 268. (c) $ReSe_2$: Alcock, N. W.; Kjekshus, A. *Acta Chem. Scand.* **1965**, *19*, 79. (d) $AuTe_2$: Tunell, G.; Ksanda, C. J. *J. Wash. Acad. Sci.* **1935**, *25*, 32. (e) $AgAuTe_4$: Tunell, G.; Pauling, L. *Acta Crystallogr.* **1952**, *5*, 375. (f) TaS_2: Brouwer, R.; Jellinek, F. *Acta Crystallog.* **1975**, *A31*, S85; *Mater. Res. Bull.* **1974**, *9*, 827. (g) $TaSe_2$ and $Ta_{1-x}Ti_xS_2$: Wilson, J. A.; D. Salvo, F. J.; Mahajan, S. *Adv. Phys.* **1975**, *24*, 117. (h) VTe_2: Bronsema, K. D.; Bus, G. W.; Wiegers, G. A. *J. Solid State Chem.* **1984**, *53*, 415.

(3) A discussion of WTe_2 and other distorted CdI_2 may be found in the following: Pearson, W. B. *The Crystal Chemistry and Physics of Metals and Alloys*; Wiley-Interscience: New York, 1972; pp 440–445.

(4) See: Hulliger, F. *Structural Chemistry of Layer-Type Phases*; Reidel: Dordrecht, Holland, 1976; pp 221–223.

(5) (a) Canadell, E.; LeBeuze, A.; El Khalifia, M. A.; Chevrel, R.; Whangbo, M.-H. *J. Am. Chem. Soc.* **1989**, *111*, 3778. (b) Buhannic, M.-A.; Ahouandjinou, A.; Danot, M.; Rouxel, J. *J. Solid State Chem.* **1983**, *49*, 77. (c) Rouxel, J. *Physica* **1980**, *99B*, 3. (d) Kertesz, M.; Hoffmann, R. *J. Am. Chem. Soc.* **1984**, *106*, 3453.

(6) See: Donohue, J. *The Structure of the Elements*; Wiley: New York, 1974.

0897-4756/89/2801-0597$01.50/0

Table II. Guinier Powder Pattern for $Ta_{0.75}Nb_{0.25}T_2$

h,k,l	d_{obs}, Å	d_{calc}, Å	I_{obs}	I_{calc}[a]
2,0,-1	8.71	8.73	vw	1.4
0,0,1	6.68	6.69	m	42.0
0,0,2	3.344	3.346	wvw	2.7
6,0,-3	2.911	2.909	ms	43.4
3,1,0	2.855	2.854	s	100.0
5,1,-1	2.554	2.553	wm	6.6
2,0,2	2.420	2.423	w	3.5
8,0,-3	2.3970	2.3974	wm	4.3
6,0,-4	2.3323	2.3317	wm	8.9
3,1-3;[b]	2.3047	2.3061	ms	36.1
6,0,0		2.3036		15.5
3,1,1	2.2918	2.2924	wm	14.1
4,0,-4;[b]		2.2360		3.4
1,1,2	2.2313	2.2338	wm	3.4
0,0,3		2.2290		9.5
5,1,0	2.2016	2.2011	vw	2.5
7,1,-3	2.1499	2.1503	w	2.6
5,1,-4	1.9545	1.9527	vw	1.6
7,1,-4	1.9356	1.9348	vw	2.1
9,1,-3	1.8458	1.8467	ms	23.4
3,1,-4	1.8278	1.8279	wm	15.7
0,2,0	1.8182	1.8193	m	17.4
8,0,0	1.7284	1.7277	vw	2.9
0,0,4	1.6718	1.6718	w	6.2
1,1,-4;[b]		1.6261	wvw	2.7
9,1,-5	1.6261	1.6238		2.5
9,1,-1	1.6091	1.6095	vw	3.1
11,1,-4	1.5767	1.5762	wvw	3.4
12,0,-5	1.5674	1.5673	vw	2.1
12,0,-3;[b]	1.5585	1.5587	w	4.7
11,1,-3		1.5579		3.1
6,2,-3	1.5431	1.5428	wm	15.4
3,1,3	1.4744	1.4748	vw	2.6
8,2,-3	1.4493	1.4493	vw	2.2
6,2,-4	1.4344	1.4343	wvw	4.8
6,2,0	1.4274	1.4277	w	8.5
0,2,3	1.4099	1.4095	vw	5.6
11,1,-6	1.3897	1.3899	vw	4.0
8,2,-1	1.3625	1.3624	vw	3.9
6,2,1	1.2882	1.2872	vw	3.7
5,1,3	1.2556	1.2558	w	7.3
0,2,4	1.2305	1.2310	wvw	6.2
12,2,-3	1.1834	1.1837	wvw	5.5
3,3,0	1.1729	1.1729	wm	11.3

[a] As calculated by the LAZY PULVERIX program of K. Yvon, W. Jeitschko, and E. Parthé, using the $NbTe_2$ atomic positional parameters. [b] Where assignment is ambiguous, the value is not used in determining cell constants.

In Tables I and II we show representative X-ray powder spectral data. The different structure types are readily assignable from such an X-ray powder study. Among the major differences are the splitting of the CdI_2 (1,0,1) reflection into the $TaTe_2$ (6,0,-3) and (3,1,0) reflections and the appearance of the $TaTe_2$ (2,0,-1), (5,1,-1), and (8,0,-3) superstructure lines. The absence of these markers together with lines indexable with a CdI_2 hexagonal cell are the criteria we used to assign a compound to the CdI_2 structure type. In Tables III and IV we report the cell parameters we obtained for the various compounds. Also shown in these tables are electron microprobe analyses of single crystals which further corroborate the homogeneity of our sample. In the $Ta_xNb_{1-x}Te_2$ system the microprobe analysis is particularly important as the variation in all parameters is small. It appears that for $Ta_xNb_{1-x}Te_2$ homogeneous phases can be prepared for all values of x ($0 \leq x \leq 1$), and that for all x values the system is in the $TaTe_2$ structure type at room temperature. Similarly for $Ta_xTi_{1-x}Te_2$, homogeneous phases could be obtained at all values of x. At the critical values $x_c = 0.85 \pm 0.02$ there is a phase transition from the $TaTe_2$ to the CdI_2 structure type. For $Ta_xZr_{1-x}Te_2$ only for $0.5 \leq x \leq 1$ were homogeneous phases observed. For $x < 0.5$ there is increasingly formation of $ZrTe_3$ and other side products. For the zirconium system, at the critical value of $x_c = 0.84 \pm 0.04$ there is a phase transition from the $TaTe_2$ to CdI_2 structure type. For $Ta_xHf_{1-x}Te_2$ a homogeneous product could be obtained only for $x > 0.875 \pm 0.025$ after which the Guinier spectrum shows it to be biphased (the second phase being a CdI_2 type $HfTe_2$ compound but with some Ta incorpo-

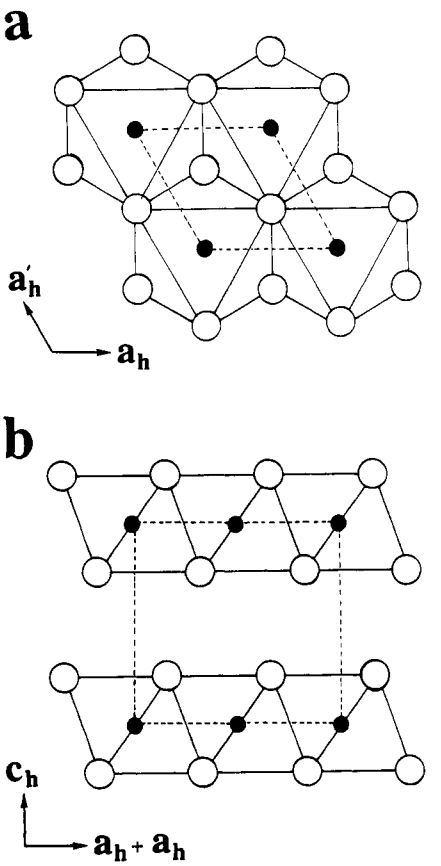

Figure 1. Hexagonal close-packed CdI_2 structure. (a) Layer of regular octahedra of anions (open circles). All the octahedra in this layer are filled by metals (closed circles). The dotted lines, which represent the unit cell, enclose the area $3^{1/2}a_h^2/2$. (b) Cross section perpendicular to the layers showing two filled layers of octahedra sandwiching an empty layer. The dotted lines indicate the nonprimitive orthorhombic cell.

Table III. $Ta_xM_{1-x}Te_2$ Phases with the $TaTe_2$ Structure Type

compd	a_m, Å	b_m, Å	c_m, Å	β_m, deg	microprobe anal.
$TaTe_2$	19.294 (6)	3.640 (1)	9.336 (5)	134.33 (2)	$Ta_{0.97(3)}Te_2$
$Ta_{0.9}Ti_{0.1}Te_2$	19.297 (4)	3.6530 (8)	9.302 (3)	134.08 (1)	$Ta_{0.88(1)}Ti_{0.07(1)}Te_2$
$Ta_{0.87}Ti_{0.13}Te_2$	19.288 (8)	3.670 (2)	9.302 (6)	133.98 (3)	
$Ta_{0.9}Zr_{0.1}Te_2$	19.321 (3)	3.6638 (8)	9.330 (2)	134.07 (1)	
$Ta_{0.875}Zr_{0.125}Te_2$	19.331 (3)	3.6698 (7)	9.336 (3)	134.01 (2)	
$Ta_{0.95}Hf_{0.05}Te_2$	19.299 (3)	3.6452 (7)	9.333 (2)	134.07 (1)	
$Ta_{0.9}Hf_{0.1}Te_2$	19.308 (6)	3.670 (1)	9.332 (4)	133.40 (2)	
$Ta_{0.75}Nb_{0.25}Te_2$	19.291 (3)	3.6386 (5)	9.334 (2)	134.24 (1)	$Ta_{0.80(5)}Nb_{0.23(1)}Te_2$
$Ta_{0.5}Nb_{0.5}Te_2$	19.326 (6)	3.6398 (6)	9.331 (3)	134.31 (2)	$Ta_{0.51(7)}Nb_{0.45(4)}Te_2$
$Ta_{0.25}Nb_{0.75}Te_2$	19.350 (8)	3.6431 (1)	9.317 (5)	134.48 (3)	$Ta_{0.21(3)}Nb_{0.72(5)}Te_2$

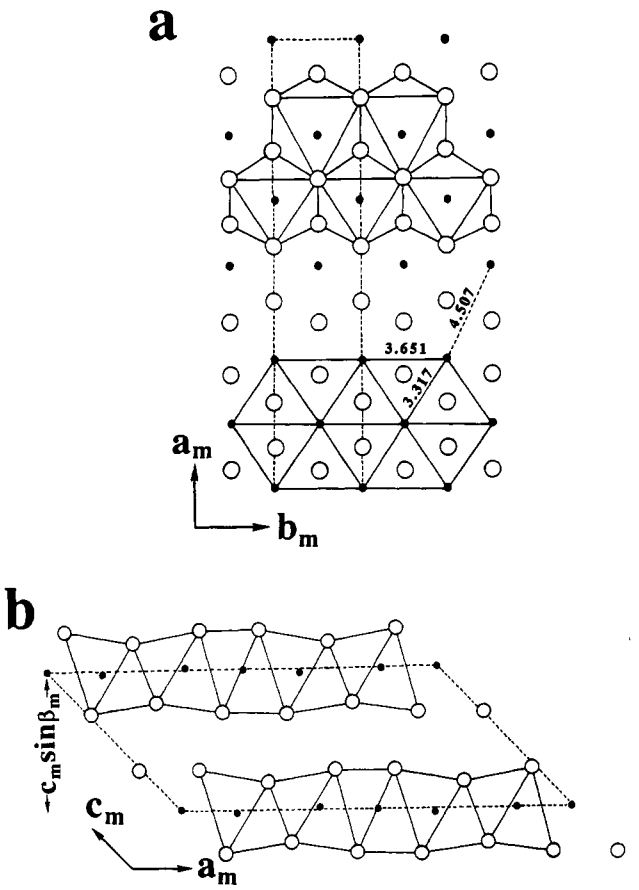

Figure 2. Monoclinic structure of $TaTe_2$ emphasizing its distortion from the CdI_2 structure type (open circles, Te; closed circles, Ta). (a) One filled layer of $TaTe_6$ octahedra. The top part shows the distorted octahedras. The bottom part indicates the triple rows of metal atoms and the shortened metal-metal bonds along this chain. The dotted lines, which indicate the unit cell, enclose the area $a_m b_m$. This corresponds to a surface area of $a_m b_m/6$ per MTe_2 unit. Compare with Figure 1a. (b) View of the structure of $TaTe_2$ similar to the one in Figure 1b, showing the displacements of metal atoms from the regular octahedral positions. The dotted lines indicate the unit cell. The interlayer spacing is $c_m \sin \beta_m$. Compare with Figure 1b.

Table IV. $Ta_xM_{1-x}Te_2$ Phases with the CdI_2 Structure Type

compd	a_h, Å	c_h, Å	c_h/a_h	microprobe anal.
$Ta_{0.83}Ti_{0.17}Te_2$	3.690 (2)	6.698 (2)	1.815	
$Ta_{0.8}Ti_{0.2}Te_2$	3.692 (1)	6.701 (1)	1.815	
$Ta_{0.7}Ti_{0.3}Te_2$	3.6951 (9)	6.711 (1)	1.816	
$Ta_{0.6}Ti_{0.4}Te_2$	3.707 (2)	6.689 (2)	1.804	$Ta_{0.60(1)}Ti_{0.36(1)}Te_2$
$Ta_{0.5}Ti_{0.5}Te_2$	3.7182 (9)	6.655 (1)	1.790	
$Ta_{0.8}Zr_{0.2}Te_2$	3.7164 (8)	6.723 (1)	1.809	$Ta_{0.90(3)}Zr_{0.13(1)}Te_2$
$Ta_{0.7}Zr_{0.3}Te_2$	3.735 (1)	6.735 (2)	1.803	$Ta_{0.83(4)}Zr_{0.17(3)}Te_2$
$Ta_{0.6}Zr_{0.4}Te_2$	3.741 (1)	6.740 (1)	1.802	$Ta_{0.65(3)}Zr_{0.26(6)}Te_2$
$Ta_{0.5}Zr_{0.5}Te_2$	3.760 (2)	6.742 (3)	1.793	

rated within it). For $x > 0.875$, only the $TaTe_2$ structure type was found. Similarly only a small percentage of V (less than 10–15%, i.e., $x > 0.85$ or 0.90) could be incorporated in the $Ta_xV_{1-x}Te_2$ system. Electron microprobe analysis shows this last system to be unusually poorly crystallized. Again only the $TaTe_2$ structure type was observed. Overall while in many cases the Guinier spectra showed only MTe_2 compounds present, for certain stoichiometries $TaTe_4$ was also found as a minor product. This side product was found consistently in $Ta_xZr_{1-x}Te_2$ with x ranging between 0.80 and 0.85. Regrinding and reannealing the samples at 1070 °C did not change the product distribution. Finally we prepared $Ta_{0.80}Zr_{0.20}Te_{1.8}$ and $Ta_{0.85}Zr_{0.15}Te_{1.8}$ under the same conditions described above. No $TaTe_4$ was observed in these metal rich samples while the other lines appeared unchanged. This indicates that for these compositions a nonstoichiometric metal-rich dichalcogenide is the product. Microprobe analysis confirms but does not prove this result.[7] Finally no oxides were detected in the Guinier powder patterns in the case of $Ta_xTi_{1-x}Te_2$.

Table V. Comparison of Miscibility to Molar Volume of the Binary Tellurides

M	% change in molar vol compared to $TaTe_2$	range for x in $Ta_xM_{1-x}Te_2$
Hf	+15.0	$1 \geq x > 0.875 \bullet 0.025$
Zr	+14.6	$1 \geq x > 0.5^a$
Ti	+2.7	$1 \geq x \geq 0$
Nb	+0.6	$1 \geq x \geq 0$
V[b]	−8.3	$1 \geq x > 0.90 \pm 0.05$

[a] The value is at least 0.5. It could be lower. See text. [b] Vanadium exists only as $V_{1.08}Te_2$. Density measurements show the anion closest packing is intact.

Discussion

The degree of allowable substitution for Ta atoms in the $Ta_xM_{1-x}Te_2$ systems may be partially rationalized by the 15% rule.[8] In Table V we compare the amount of miscibility between $TaTe_2$ and MTe_2 to the volume per atom of the dichalcogenides. It may be seen that both $HfTe_2$ and $ZrTe_2$ lie near the limit allowed by the 15% rule and that furthermore the two systems have entirely different miscibilities. We note that were one to apply the 15% rule rigidly, the experimental result that two metals as chemically similar as Zr and Hf behave differently would imply that the systems must lie on the border of permissible compounds. Furthermore, it may be seen that VTe_2 is significantly smaller than $TaTe_2$ and similarly has only a small solubility. However, as we show below, no argument based on atomic size accounts for the critical x value for which $Ta_xM_{1-x}Te_2$ systems distort from the CdI_2 to the $TaTe_2$ structure type.

To study this distortion, it is most convenient to transform the four monoclinic parameters (a_m, b_m, c_m, and β_m) into two sets of two parameters. The first two parameters are unitless and measure the degree of the monoclinic distortion of the original hexagonal CdI_2 cell. The first, $a_m/3(3^{1/2})b_m$, measures the elongation within a given layer, the second, $|a_m/3c_m \cos \beta_m|$, measures the slippage between layers. For truly hexagonal compounds both distortion parameters equal 1. The final two parameters are $a_m b_m/6$ and $c_m \sin \beta_m$. These parameters measure respectively the average surface area occupied by each MTe_2 unit and the interlayer spacing (see Figure 2). The equivalent hexagonal parameters are $3^{1/2}a_h^2/2$ and c_h. We plot both these latter parameters and their hexagonal equivalents for both the $Ta_xTi_{1-x}Te_2$ and $Ta_xZr_{1-x}Te_2$ systems in Figures 3 and 4. It may be seen that there is no noticeable kink in any of the four curves near the critical value x_c at which the structural transformation occurs.[9] The phase transition (as a function of compo-

(7) Microprobe analyses for $Ta_{0.85}Zr_{0.15}Te_2$ and $Ta_{0.8}Zr_{0.2}Te_2$ give a combined metal to tellurium ratios of $M_{1.04(4)}Te_2$ and $M_{1.03(3)}Te_2$. For $Ta_{0.9}Zr_{0.1}Te_2$, $Ta_{0.75}Zr_{0.25}Te_2$, $Ta_{0.7}Zr_{0.3}Te_2$, and $Ta_{0.65}Zr_{0.35}Te_2$ respective ratios of $M_{0.98(15)}Te_2$, $M_{0.94(5)}Te_2$, $M_{1.00(4)}Te_2$, and $M_{0.97(2)}Te_2$ were found. Furthermore in these last four cases either no or trace amounts of $TaTe_4$ were found.

(8) See discussion in Hansen, P. *Physical Metallurgy*, 2nd ed.; Cambridge University Press: Cambridge, 1986; pp 136–144. The 15% rule is an approximate rule that states that extensive solubility of one element with another occurs most often when the elemental size is within 15% of one another.

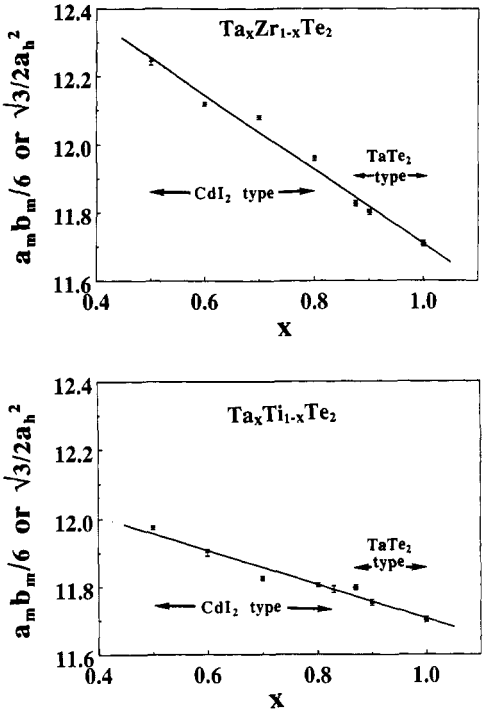

Figure 3. Plot of the composition vs the average surface occupied by each MTe_2 unit in $Ta_xM_{1-x}Te_2$ (M = Ti or Zr). $a_m b_m/6$ is for the distorted $TaTe_2$ structure type, and $3^{1/2}a_h^2/2$ is the corresponding parameter for the undistorted CdI_2 structure type. Error bars are $\pm 1\sigma$.

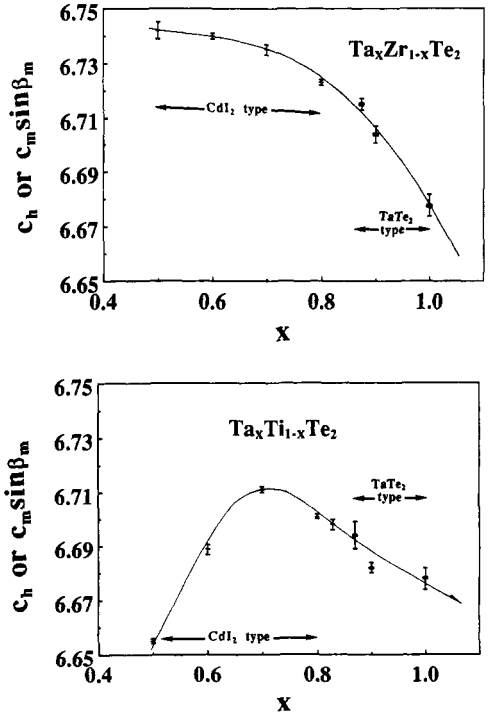

Figure 4. Variation of the interlayer spacing as a function of x for $Ta_xM_{1-x}Te_2$ (M = Ti or Zr). c_h is the functional form used for the CdI_2 structure type, and $c_m \sin \beta_m$ for the $TaTe_2$ structure type. Error bars are $\pm 1\sigma$.

sition) is therefore accompanied by neither a measurable density nor surface area discontinuity.

We now turn to the distortion parameters described above. We plot the value of $a_m/3(3^{1/2})b_m$ for $Ta_xM_{1-x}Te_2$ systems in Figure 5, with Figure 5a showing the values for

(9) The $TaTe_2$ structure type forms a subgroup of the 1T structure type. See Figures 1 and 2.

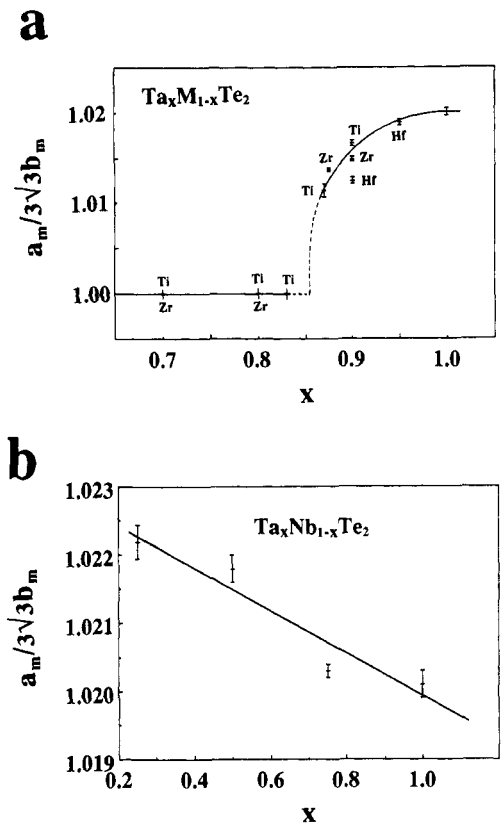

Figure 5. Elongation distortion parameter as a function of x for $Ta_xM_{1-x}Te_2$. (a) Distortion parameter for M = Ti, Zr, and Hf. Error bars are $\pm 1\sigma$. (b) The same for M = Nb.

M = Ti, Zr, and Hf and Figure 5b those for M = Nb. It may be seen for the materials plotted in Figure 5a that to a surprising degree the $a_m/3(3^{1/2})b_m$ parameter depends principally on the x value and not on the constituent M atoms. This is true despite the very different sizes of the Ti or Zr atoms. It is possible to relate this result to the earlier result which indicated that the $TaTe_2$ to CdI_2 transition occurred without a significant change in surface area or density. The argument is as follows.[10] Suppose that a decrease in density were observed in going from $TaTe_2$ to CdI_2 structure types. Hence a decrease in pressure would favor the CdI_2 type. The substitution would have just such a "negative pressure" effect and therefore would help induce a transformation from the $TaTe_2$ to the CdI_2 type. Conversely, the absence of a change in density would by the same argument result in an insensitivity to the size of substituting metal atoms. This latter result is what we observe.

In comparing the results of Figure 5a with those of Figure 5b, we see that while size factors are not important, changes in electron number are significant. The two curves in Figure 5 are entirely different. Indeed there does not appear to be any decrease in the distortion parameter for any value of x in $Ta_xNb_{1-x}Te_2$. The most obvious difference between the Nb and the Ti, Zr, or Hf systems is that for all x values, the $Ta_xNb_{1-x}Te_2$ is isoelectronic with $TaTe_2$ or $NbTe_2$. This is not the case for Ti, Zr, or Hf. Finally the curve in Figure 5b gives us some measure of the importance of cation site disorder. Were such disorder to play a prominent role, we ought to find an arched shape to the $a_m/3(3^{1/2})b_m$ curve in going from the ordered $TaTe_2$

(10) Such an argument based on the pressure induced by dopaing has been used to account for the phase transition found in the $Gd_xSm_{1-x}S$ systems. See: Jayaraman, A.; Bucher, E.; Dernier, P. D.; Longinotti, L. D. *Phys. Rev. Lett.* **1973**, *31*, 700.

to the ordered $NbTe_2$. Such a bend is not observed. Therefore, at least for the case of $TaTe_2$ and $NbTe_2$, cation disorder is not a significant structural factor.

It is informative to compare our results with the earlier work of Wilson et al.[2g] on the $13^{1/2}a_0$ distortion present in TaS_2 and $TaSe_2$. In their work they studied the $Ta_xM_{1-x}S_2$ (M = Ti, Nb), $Ta_xM_{1-x}Se_2$ (M = Ti, V), and TaS_ySe_{2-y} systems. Their work shows that for metal doping the distortion is lost for x_c values ranging from 0.95 to 0.90. A much weaker effect is observed for the TaS_ySe_{2-y} systems. They concluded that this was due to a weaker effect for anion as opposed to cation disorder. However, it should be noted that the TaS_ySe_{2-y} system is the only one in which both antipodes (i.e., TaS_2 and $TaSe_2$) are in the $13^{1/2}a_0$ distortion type. In our work, again there are two binary systems that have the $TaTe_2$ distortion ($TaTe_2$ and $NbTe_2$), but for our system the two differ in their cations. It therefore appears that the principal factor governing the stability of the various distortion modes is not cation or anion disorder, not size factors, and not solely d-electron counts (for TaS_2 and $TaTe_2$ are isoelectronic) but instead merely whether the two antipodes belong to the same distortion type.[11]

Finally it should be recalled that the $TaTe_2$ distortion is formed by a commensurate charge density wave.[12] Our work therefore studies the effect of dopants on commensurate charge density wave formation (which is quite different from the effect expected for incommensurate charge density waves[13]). Of special interest are our results for the $Ta_xNb_{1-x}Te_2$ solution. Our results indicate that disorder on the metallic sites need not eliminate the commensurate charge density wave (irrespective of the impurity concentration). This is in contrast to the theoretical results of Baeriswyl,[14] which indicate for one-dimensional commensurate charge density waves that the distortion will be suppressed at high impurity concentration. It is of interest that Baeriswyl's predictions are exactly borne out in the *one*-dimensional commensurate charge density wave (Peierl's distortion) found in $Ta_{1-x}Nb_xO_2$.[15] Perhaps the higher dimensionality of the $TaTe_2$ distortion (two dimensional) plays a role in the differing effects. For other high-dimensional distortions, impurities are also known to cause weaker effects. For example, the three-dimensional distortion found in elemental Se and Te is found for the full range of Se_xTe_{1-x} solutions.[16]

Recent work of Tremel[17] using the extended Hückel method has shown that the forces during the distortion are electronic in nature. Our current work has studied the effect that disorder has on the $TaTe_2$ distortion. We have found that it is the electronic effects brought about by disorder that are of primary importance and not the steric effects brought about by disorder.

(11) However, when the antipodes are different, our results indicate cation substitution (with change in electron count) have a stronger effect than anion substitution (without change in electron count). For example, $TaTe_ySe_{2-y}$ is known to be in the $TaTe_2$ structure type for all $y > 1$ (this result is presented in: Antonova, E. A.; Kiseleva, K. V.; Medvedev, S. A. *Sov. Phys. JETP* **1971**, *32*, 31).

(12) (a) See: *Charge Density Waves in Solids*; Hutiray, Gy., Sólyom, J., Eds.; Springer-Verlag: Berlin, 1985. (b) Whangbo, M.-H.; Canadell, E. *J. Am. Chem. Soc.* **1988**, *110*, 358. Whangbo, M.-H.; Canadell, E.; Schlenker, C. *J. Am. Chem. Soc.* **1987**, *109*, 6308.

(13) See discussion in: *Basic Notions of Condensed Matter Physics*; Anderson, P. W., Ed.; Benjamin: Menlo Park, CA, 1984; pp 99–101.

(14) Baeriswyl, D. In *Theoretical Aspects of Band Structure and Electronic Properties of Pseudo-One Dimensional Solids*; Kamimura, H., Ed.; Reidel: Dordrecht, Holland, 1985; pp 35–38.

(15) Morawietz, J. *J. Inorg. Nucl. Chem.* **1966**, *28*, 941.

(16) (a) The Se distortion is discussed in: Burdett, J. K.; Lee, S. *J. Am. Chem. Soc.* **1983**, *105*, 1079. (b) Te_xSe_{1-x}: Smorodina, T. P. *Sov. Phys. Sol. State (Eng. Trans.)* **1960**, *2*, 807.

(17) Tremel, W., to be published.

Physical and Electrical Characterization of Poly[bis((methoxyethoxy)ethoxy)phosphazene]–Metal Polyiodide Complexes

M. M. Lerner, L. J. Lyons, J. S. Tonge, and D. F. Shriver*

Department of Chemistry and Materials Research Center, Northwestern University, 2145 Sheridan Road, Evanston, Illinois 60208-3113

Received June 27, 1989

Complexes of poly[bis((methoxyethoxy)ethoxy)phosphazene] (MEEP = $[NP(OC_2H_4OC_2H_4OCH_3)_2]_p$) with alkali-metal polyiodide salts were prepared by the reaction of solid $MEEP_xMI$ with I_2 vapor. The compositional range $MEEP_xMI_n$ (x = 16–2, n = 1–9, M = Li, Na) was systematically characterized by Raman spectroscopy, differential scanning calorimetry, and electrical measurements. In addition, a number of complexes with higher iodine content (up to 80 wt %), with n = 11–23, as well as salt-free MEEP–I_2 complexes were examined. Triiodide and polyiodide species are observed in all complexes except for n = 1; molecular I_2 is not present in any of the complexes prepared. At lower iodine contents (n = 1–9) conductivity increases with salt concentration until x = 4 and also increases steadily with higher iodine content. At high polyiodide concentrations conductivities are as high as 5×10^{-3} S cm^{-1} at 30 °C. In conventional polymer–salt complex electrolytes, cation and anion diffusion is enabled by polymer segmental motion. Polyiodide complexes, however, appear to be relatively insensitive to polymer dynamics, and the conduction process is thought to involve iodide transfer between polyanions.

Introduction

The study of ion-conducting polymers has been active during the past decade.[1,2] These materials can retain the advantages of polymers (such as processability) and possess useful electrical properties for solid-state devices. Applications for these materials depend upon factors such as

(1) MacCallum, J. R., Vincent, C. A., Eds. *Polymer Electrolyte Reviews 1*; Elsevier Applied Science: London, England, 1987.

(2) Tonge, J. S.; Shriver, D. F. In *Polymers for Electronic Applications*; Lai, J., Ed.; CRC Press: Boca Raton, FL, 1989, and references therein.

0897-4756/89/2801-0601$01.50/0